Journal of Catalysis **198,** 195–207 (2001)
doi:10.1006/jcat.2000.3120, available online at http://www.idealibrary.com on IDEAL®

Partial Oxidation of Methane to Synthesis Gas over Ru/TiO_2 Catalysts: Effects of Modification of the Support on Oxidation State and Catalytic Performance

C. Elmasides,* D. I. Kondarides,* S. G. Neophytides,† and X. E. Verykios*,[1]

*Department of Chemical Engineering, University of Patras, GR-26500 Patras, Greece; and †Institute of Chemical Engineering and High Temperature Chemical Processes (ICE/HT-FORTH), P.O. Box 1414, GR-26500 Patras, Greece

Received June 5, 2000; revised November 23, 2000; accepted November 23, 2000; published online February 13, 2001

The effects of modification of the support on the oxidation state of Ru and the catalytic performance of Ru/TiO_2 catalysts under conditions of partial oxidation of methane to synthesis gas have been investigated employing XPS and FTIR techniques. It has been found that the oxidation state of Ru depends on the reaction temperature and on the supporting material and that, under conditions where the direct reaction route is operable, the catalytic performance (conversion of methane and selectivity toward synthesis gas formation) is improved over samples that mainly contain Ru in its metallic form. Doping of TiO_2 with small amounts of W^{6+} cations favors oxygen adsorption on Ru under reaction conditions, thus resulting in stabilization of a fraction of the catalyst in its oxide forms. This is reflected in lower activity and selectivity of this catalyst compared to those of the undoped one. In contrast, Ru supported on undoped and Ca^{2+}-doped TiO_2 exists mainly in the metallic form and, as a result, it promotes the direct conversion of methane to synthesis gas. *In situ* **FTIR spectroscopy showed that an adsorbed CO species exists on the surface of the latter two catalysts under reaction conditions, even at temperatures as high as 1073 K. This species, which is not observable over the W^{6+}-doped catalyst, is related to a Ru surface site, which is responsible for the dissociation of methane and formation of CO.**

1. INTRODUCTION

Several attempts have been made in recent years to achieve synthesis gas formation via catalytic partial oxidation of methane (CPO) (1). Compared to steam reforming, which is the dominant commercial method employed to produce synthesis gas, the direct oxidation of methane is more energy efficient and can produce a more desirable H_2/CO ratio, required for methanol or Fischer–Tropsch synthesis (1). However, the direct oxidation reaction has not been developed at industrial scale because it involves cofeeding of CH_4 and O_2 under flammable or even explosive conditions. Moreover, local hot spots may be formed within catalyst beds, which can irreversibly damage the active ingredient of the catalyst or even the reactor. Hence, knowledge of the reaction mechanism and, especially, understanding of the nature of active surface sites that participate in reaction steps can lead to the development of appropriate catalysts for industrial usage.

Concerning the reaction pathway of partial oxidation of methane, two alternative routes have been proposed: (a) a sequential scheme according to which the initial total oxidation of methane is followed by reformation of the unconverted methane with CO_2 and H_2O (indirect scheme) and (b) the direct conversion of CH_4 to synthesis gas (H_2 and CO), which does not involve the formation of CO_2 and H_2O as reaction intermediates (direct scheme).

The catalytic partial oxidation of methane has been studied on noble metals, such as Rh, Ru, Pd, and Pt in unsupported (2–5) or supported form (6–8) and on supported Ni catalysts (9, 10). It is generally agreed that the type of catalyst employed may strongly influence the reaction steps of the catalytic partial oxidation of methane. Mallens *et al.* (2) have studied the partial oxidation of methane to synthesis gas over Rh and Pt catalysts and found differences in the selectivity toward CO and H_2. These differences were attributed to the lower activation energy of methane decomposition on Rh than on Pt. The authors support the view that the ability of the catalyst to activate methane determines the concentration of active surface species such as oxygen, carbon, and hydrogen and, consequently, product distribution. Fathi *et al.* (3) have also studied Pt catalysts for the partial oxidation of methane and proposed that product distribution is determined by the kind and concentration of surface oxygen species. For supported metal catalysts, the choice of the support may also influence the concentration of adsorbed oxygen and, consequently, the activation of methane and product distribution (6).

Previous investigations in this laboratory have shown that Ru supported on TiO_2 exhibits unique performance by catalyzing the direct reaction scheme, to an appreciable extent, at relatively low reaction temperatures (11, 12). More

[1] To whom correspondence should be addressed. Fax: +30-61-991 527. E-mail: verykios@chemeng.upatras.gr.

0021-9517/01 $35.00

specifically, it has been found that, in the absence of significant mass and heat transfer resistances, high selectivity to synthesis gas (>60%) is obtained over Ru/TiO_2 catalysts in the low methane conversion range (oxygen conversion <100%) at temperatures as low as 873–973 K. On the other hand, very low selectivity to synthesis gas in the presence of oxygen is obtained, over other metal catalysts (Ni, Rh, Pd and Ir) as well as over Ru catalysts supported on carriers other than TiO_2 (12). This has been attributed to the ability of the TiO_2 carrier to stabilize Ru in its reduced state, thus inhibiting oxidation of the catalyst under conditions of partial oxidation of methane (13). In the present study, the effects of modification of TiO_2 by doping with Ca^{2+} or W^{6+} cations on the oxidation state of supported Ru has been investigated by XPS and FTIR. The results obtained are related to the catalytic performance of Ru supported on modified TiO_2 carriers under conditions of partial oxidation of methane to synthesis gas.

2. EXPERIMENTAL PROCEDURES

2.1. Catalyst Preparation

TiO_2 carriers doped with 0.95 at.% Ca^{2+} or 0.68 at.% W^{6+} were prepared by the method of high-temperature diffusion of the dopant cation into the crystal matrix of titania. The parent TiO_2 carrier used in the present study was Degussa P25 (specific surface area: 50 ± 2 m^2/g) and the precursors used for the preparation of the W^{6+}- and Ca^{2+}-doped carriers were WO_3 and CaO, respectively, obtained from Alfa Products. In the final step of preparation of the doped carriers, materials were calcined in air at 1173 K for 5 h. For comparison purposes, and to produce materials with similar physical characteristics, undoped TiO_2 was calcined at 973 K for 5 h. The specific surface area of the doped and undoped carriers was measured with the BET technique, employing nitrogen physisorption at the temperature of liquid nitrogen.

Ru catalysts, with a metal loading of 0.5 wt%, were prepared by employing the incipient wetness impregnation method, using $Ru(NO)(NO_3)_3$ (Alfa Products) as the starting material. After preparation, all catalysts were reduced in flowing H_2 at 573 K for 2 h and then stored in sealed vials until further use. Catalysts were characterized in terms of metal dispersion, employing hydrogen chemisorption at room temperature. Monolayer coverages were estimated by extrapolation of the linear part of the H_2 chemisorption isotherms to zero pressure.

2.2. Catalytic Performance Tests

The catalytic performance of supported Ru catalysts for the partial oxidation of methane to synthesis gas was studied in a continuous flow reactor in the temperature range of 973–1073 K. Experiments were conducted using dilute feed mixtures consisting of $CH_4/O_2/N_2$ (6/3/91 vol%). The reactor employed consists of a quartz tube (6-mm O.D.), with an enlargement (8 mm O.D.) at its central part where the catalyst is placed. The catalyst bed is supported by means of quartz wool. The quantity of catalyst used in these experiments varied between 10 and 30 mg and the particle size was in the range of 0.12–0.18 mm. A K-type thermocouple enclosed in a quartz well (3-mm o.d.) was positioned inside the catalyst bed for accurate measurement of the catalyst bed temperature. The total feed flow rate was in the range of 400–1000 cm^3 (STP)/min.

Two gas chomatographs were used for the analysis of reactants and products. CH_4 and CO_2 were separated in a Carboxen 1000 column and O_2, N_2, and CO in a molecular sieve 5A column with He as the carrier gas. Hydrogen was analyzed in the second chromatograph, employing N_2 as the carrier gas. H_2O produced during the reaction was condensed downstream of the reactor.

2.3. XPS Experiments

XPS experiments were carried out with a SPECS LHS 10 spectrometer, employing the Mg $K\alpha$ exciting radiation (1253.6 eV). The X-ray source was operated at 15 kV–20 mA and the kinetic energy of the photoelectrons was measured by the hemispherical electron analyzer in the pass-energy mode (36 eV). The sample, which was mounted on a transfer rod probe, could be easily transferred from the atmospheric pressure chamber, where it could be treated with gases at atmospheric pressure and elevated temperatures (up to 973 K), to the UHV chamber. During pretreatment of the catalyst sample under reaction gas mixture, on-line analysis of the effluent gas was possible by means of a mass spectrometer (Omnistar) connected at the exit of the pretreatment chamber.

XP spectra were obtained in the binding energy (BE) regions of Ti(2*p*), Ru(3*d*), C(1*s*), and O(1*s*) lines. Since the C(1*s*) signal is superimposed with the Ru(3*d*) signal, the main line of the support (Ti(2*p*) at 458.7 eV) was taken as a secondary reference. Signal shape analysis for the Ru(3*d*)/C(1*s*) region was performed with the program package Xpspeak. Binding energies and full width at half maximum (FWHM) were kept constant in a narrow range of admitted deviations. The Ru(3*d*) spin–orbit coupling energy (difference between the BE of Ru($3d_{3/2}$) and Ru($3d_{5/2}$)) was kept at 4.10 ± 0.05, while the area ratio of these components was kept at 0.65 ± 0.05 (13). Atomic ratios of elements were calculated by integration of the XPS signals in preselected BE windows, employing a Shirley-type background.

2.4. FTIR Spectroscopy

A Nicolet 740 FTIR spectrometer equipped with a DRIFT cell, an MCT detector, and a KBr beamsplitter was used in the present study. For all spectra, a 64-scan data

acquisition was carried out at a resolution of 4.0 cm^{-1}. The apparatus and procedures for obtaining *in situ* FTIR spectra have been described in detail elsewhere (13).

CO adsorption was studied at room temperature (RT) over samples pretreated at selected conditions, i.e., after treatment with oxygen, hydrogen, or a $CH_4/O_2/Ar$ mixture. *In situ* FTIR spectra were also recorded at reaction conditions in the temperature range of 773 to 1073 K. In these experiments, each sample was first reduced in flowing hydrogen (20% H_2 in Ar) at 773 K for 60 min and then the gas phase was purged by switching to Ar flow, at 773 K, for 10 min. After the purging process, the flow was switched to the reaction mixture and spectra were recorded after ca. 30 min on stream when steady state conditions were reached. Subsequently, the sample was heated at a higher reaction temperature under flow of the reaction mixture, and the next spectrum was recorded when the new reaction temperature had stabilized.

3. RESULTS

3.1. Catalysts Characterization

The morphological characteristics of the catalysts examined are summarized in Table 1. It is observed that the high-temperature pretreatment of the doped and undoped carriers results in reduction of the specific surface area of the parent TiO_2 material from 50 to 11–15 m^2/g and in complete transformation of the oxide to its rutile form. According to the H_2 chemisorption results, the dispersion of Ru is somewhat higher over the doped samples than over the undoped one, and the average crystallite size is ca. 2 nm.

3.2. Kinetic Experiments

Several sets of experiments have been carried out in the temperature range of 973 to 1073 K to evaluate the kinetic behavior of the three Ru catalysts. Typical results, obtained over Ru/TiO_2, $Ru/TiO_2(Ca^{2+})$, and $Ru/TiO_2(W^{6+})$ catalysts at 1073 K, are presented in Fig. 1, in which selectivities toward CO (S_{CO}) and H_2 (S_{H_2}) are shown as functions of CH_4 conversion (X_{CH_4}). In all cases, two distinct regions can be observed: one for $X_{CH_4} < 35\%$, where S_{CO} and S_{H_2} remain constant, and one for $X_{CH_4} > 35\%$, where selectivities toward both products increase with increasing methane conversion. It is important to note that, in the first region ($X_{CH_4} < 35\%$), analysis of the gas at the effluent of the reactor shows that oxygen is not fully consumed ($X_{O_2} < 100\%$) and it varies between 10 and 90%. In this region, selectivities toward both CO and H_2 depend strongly on the nature of the support (Fig. 1): Doping TiO_2 with Ca^{2+} cations results in increased selectivities while the opposite is true upon doping TiO_2 with W^{6+} cations. The activity of the catalysts was also found to depend on the carrier and to follow a pattern similar to that of selectivity; i.e., the Ca^{2+}-doped catalyst exhibits highest activity while the W^{6+}-doped catalyst the lowest (Table 2). It is also apparent from the results reported in Table 2 that selectivity toward CO and H_2 formation in the presence of oxygen increases significantly with increasing temperature.

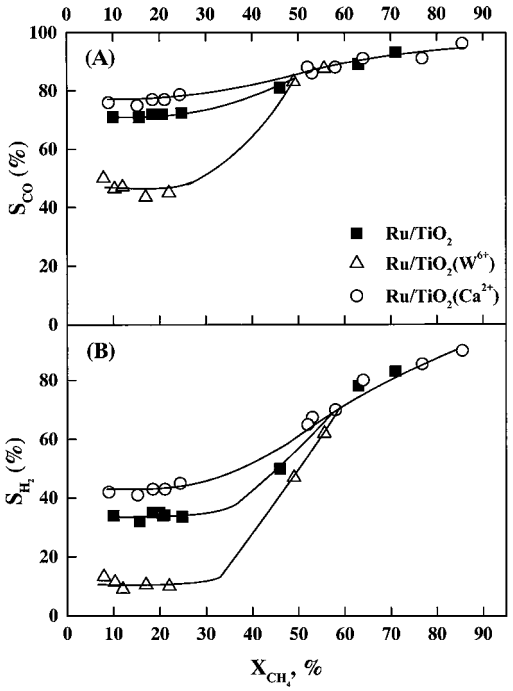

FIG. 1. Selectivities toward CO (S_{CO}) and H_2 (S_{H_2}) formation, obtained over the Ru catalysts, as functions of methane conversion (X_{CH_4}). $T = 1073$ K; feed composition: 6%CH_4–3%O_2 (in N_2).

It should be noted that, in all experiments where methane conversion is less than 100%, S_{CO} is essentially independent of space velocity and that selectivity toward CO formation is improved upon doping TiO_2 with Ca^{2+} while it is significantly reduced upon doping TiO_2 with W^{6+} cations. A qualitatively similar behavior was observed over a wide temperature range (973–1073 K).

3.3. XPS Spectra of Supported Ru Catalysts at Reaction Conditions

XPS spectra obtained in the Ru(3*d*) region from the unmodified Ru/TiO_2 catalyst are shown in Fig. 2A. It is

TABLE 1

Morphological Characteristics of the Ru Catalysts

	Ru/TiO_2	$Ru/TiO_2(Ca^{2+})$	$Ru/TiO_2(W^{6+})$
Specific surface area ($m^2\ g^{-1}$)	11	12	15
Ru dispersion (%)	34	50	56
Ru particle size (Å)[a]	26	18	16
Crystalline mode of the support	Rutile	Rutile	Rutile

[a] Calculated from metal dispersion, assuming spherical particles.

TABLE 2

Results of Activity and Selectivities toward CO (S_{CO}) and H_2 (S_{H_2}) Formation at Different Reaction Temperatures under Conditions of Low Oxygen Conversion

Reaction temp. (K)	Ru/TiO_2			$Ru/TiO_2(Ca^{2+})$			$Ru/TiO_2(W^{6+})$		
	[a] R_{CH_4} (mol g^{-1} s^{-1})	S_{CO} (%)	S_{H_2} (%)	[a] R_{CH_4} (mol g^{-1} s^{-1})	S_{CO} (%)	S_{H_2} (%)	[a] R_{CH_4} (mol g^{-1} s^{-1})	S_{CO} (%)	S_{H_2} (%)
973	8.0×10^{-5}	61	27	8.9×10^{-5}	70	35	6.8×10^{-6}	30	6
1023	10.1×10^{-5}	64	31	11.6×10^{-5}	75	37	8.1×10^{-6}	37	9
1073	11.9×10^{-5}	71	34	14.9×10^{-5}	81	42	1.4×10^{-5}	45	11

[a] The rate of CH_4 consumption refers to the region where $X_{CH_4} < 10\%$.

observed that the spectrum obtained following reduction of the fresh catalyst with 20% H_2/Ar at 773 K (trace a) consists of a doublet with a Ru($3d_{5/2}$) BE of 280.0 eV, characteristic of metallic ruthenium (Ru(0)) (13, 14). The constraints used in the spectral analysis regarding the area ratio of the Ru($3d_{5/2}$) and Ru($3d_{3/2}$) peaks and their BE difference resulted in a satisfactory fitting of the signal shape only when a second doublet, with a Ru($3d_{5/2}$) BE of 281.1 eV, and a contribution from C(1*s*) at 284.6 eV (13) were also taken into account. The second doublet is attributed to Ru(II) species (15).

The sample was then heated under He flow to 673 K and was subsequently exposed to a 10%CH_4–5%O_2 (in Ar) mixture for 15 min (Fig. 2A, trace b). It is observed that the contributions of Ru(II) and C(1*s*) signals increase in intensity compared to those of the H_2-treated sample and that an additional ruthenium doublet with a BE of 283.4 eV is required for the satisfactory fitting of the signal shape. This doublet is attributable to Ru(IV) species (15). Results of on-line mass spectrometry obtained at the exit of the pretreatment chamber are summarized in Table 3. It is observed that, at 673 K, conversion of CH_4 is low (8%), with CO_2 and H_2O being the only reaction products.

Subsequent treatment of the Ru/TiO_2 catalyst with the CH_4–O_2 mixture at 823 K (trace c) results in an increase of the relative intensity of the Ru(0) signal at the expense of Ru(II) and Ru(IV) signals. Under these conditions, the conversion of CH_4 increases to 33% and CO appears in the gas phase (Table 3). At the reaction temperature of 973 K, Ru is fully reduced (trace d) and conversion of methane and selectivity toward CO further increase to 42% and 74%, respectively (Table 3). In addition to the progressive reduction of the catalyst, increasing the reaction temperature results in a significant increase of the intensity of the C(1*s*) signal (Fig. 2A, b,c).

The corresponding spectra obtained from the Ca^{2+}-doped catalyst are shown in Fig. 2B. It is observed that the spectra are qualitatively similar to those obtained from the undoped catalyst (compare with Fig. 2A). However, the relative intensity of the C(1*s*) peak is lower in the present case under all experimental conditions employed. In addition, small amounts of Ru(II) are detectable following treatment at 973 K (trace d). Under these conditions, the Ca^{2+}-doped catalyst is more active ($X_{CH_4} = 59\%$) and more selective ($S_{CO} = 81\%$) than the undoped one (Table 3).

In contrast, XPS spectra obtained from the W^{6+}-doped catalyst are significantly different (Fig. 2C). While after H_2 pretreatment of the W^{6+}-doped catalyst the largest portion of Ru is in the metallic state (trace a), relatively large amounts of Ru exist in oxidized forms at reaction conditions (traces b–d). In these spectra, the contribution of Ru(IV) is clearly necessary for the satisfactory fitting of the signal shapes, even at the temperature of 823 K. The differences in the oxidation state of ruthenium under reaction conditions are also reflected in the catalytic behavior of the W^{6+}-doped catalyst, which is less active and less selective compared to the undoped and the Ca^{2+}-doped catalysts (Table 3). In addition, the relative intensity of the C(1*s*) peak is much lower over the present catalyst. This is better observed in Fig. 3 in which the C/Ru atomic ratios calculated from the XPS spectra of the examined catalysts are plotted as functions of reaction temperature. It is observed that significant quantities of carbon are deposited on the undoped catalyst, the amount of which increases with increasing reaction temperature, especially at temperatures above 823 K. The C/Ru atomic ratio is small and nearly independent of temperature for the W^{6+}-doped catalyst, while it takes intermediate values for the Ca^{2+}-doped sample. It is worth noticing that under reaction conditions the carbon signal on the Ca^{2+}-doped sample appears at a higher binding energy (ca. 0.7 eV) compared to the carbon deposits on the W^{6+}-doped and undoped catalysts (Fig. 2, traces c, d). As will be further discussed, the carbon detected on the Ca^{2+}-doped sample may be attributed to stable CH_x species (16, 17) created on the surface during the dissociative adsorption of methane on the Ru/TiO_2 (Ca^{2+}) catalyst.

3.4. FTIR Experiments

3.4.1. CO adsorption on fresh and spent catalysts. The oxidation state of the Ru catalysts was also investigated by

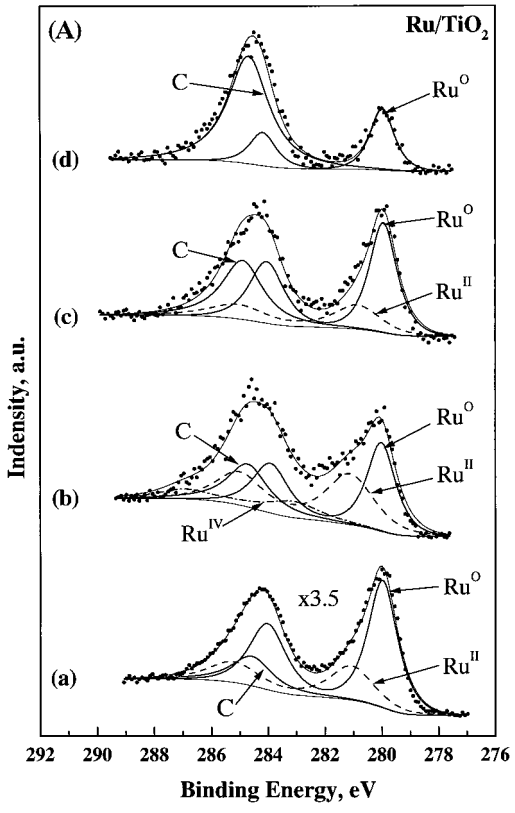

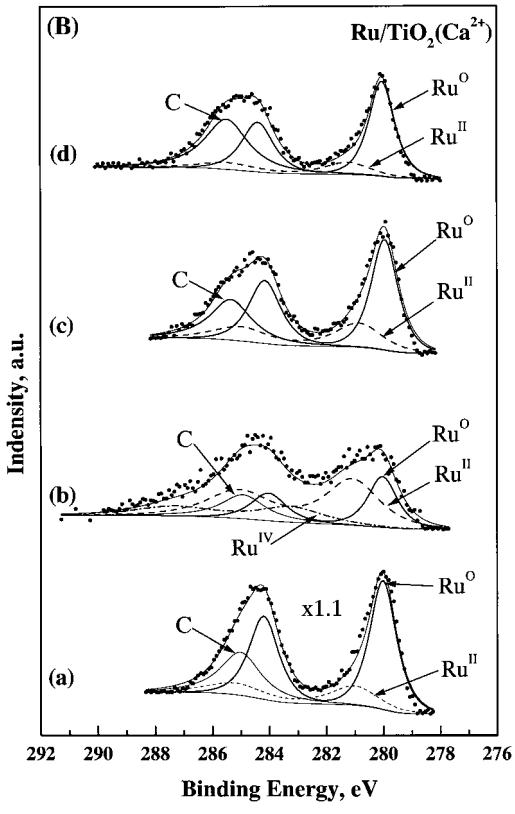

FIG. 2. XPS spectra obtained from (A) Ru/TiO$_2$, (B) Ru/TiO$_2$(Ca^{2+}), and (C) Ru/TiO$_2$(W^{6+}) catalysts after reduction with H$_2$ at 773 K for 20 min (a) following treatment with a 10%CH$_4$–5%O$_2$ (in Ar) mixture at 673 K (b), 823 K (c), and 973 K (d).

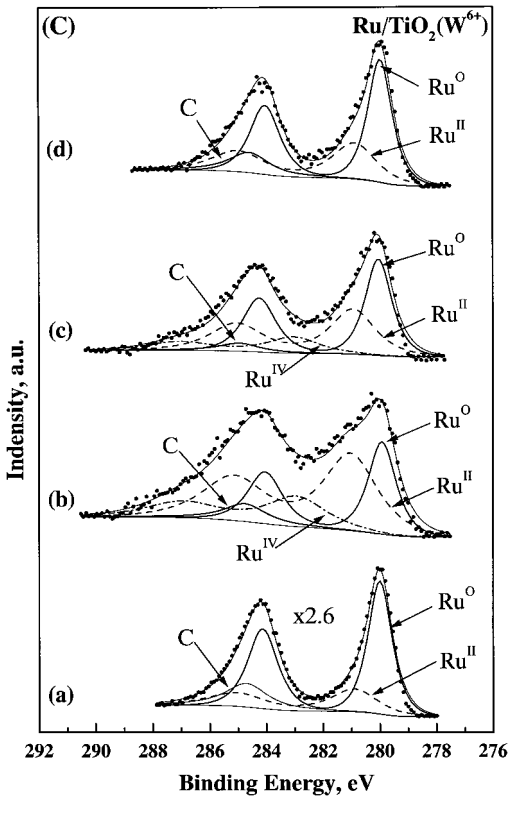

FIG. 2—*Continued*

monitoring CO adsorption at 298 K over samples previously treated with a 10%CH$_4$–5%O$_2$ (in Ar) mixture at 773 and 973 K. For comparison, similar spectra were also obtained over H$_2$-reduced and partially oxidized samples. In the latter case, the samples were treated with oxygen (7%O$_2$ in Ar) under mild conditions, i.e., at 473 K for 10 min. Results obtained from the Ru/TiO$_2$, Ru/TiO$_2$(Ca^{2+}), and Ru/TiO$_2$(W^{6+}) catalysts are presented in Figs. 4A–4C, respectively.

The FTIR spectrum obtained following exposure of the H$_2$-reduced Ru/TiO$_2$ catalyst to 7% CO for 15 min at RT is shown in Fig. 4A, trace a. Several bands due to the adsorbed CO species can be observed in the ν(C–O) region, located at 2135, 2070(sh), and 2043 cm^{-1} while a broad spectral feature may also be distinguished as a low-frequency "tail" of the 2043-cm^{-1} band. The band located at 2043 cm^{-1} may be safely attributed to CO linearly adsorbed on reduced metal crystallites (Ru^0–CO) (18). This has also been confirmed in our previous study (13) based on the frequency dependence of this peak to surface coverage. Peaks at 2135 and 2070 cm^{-1} appear at frequencies where multicarbonyls on oxidized Ru sites [Ru^{n+}(CO)$_x$, $n = 2$ or 3, $x = 2$ or 3] are expected to absorb (19–21). These peaks most probably originate from two different multicarbonyl species adsorbed on isolated oxidized Ru^{n+} sites (13). It is, however, possible that part of the 2070-cm^{-1} band corresponds to Ru^{n+}–CO monocarbonyl. For example,

TABLE 3

Conversion of Methane (X_{CH_4}) and Selectivity toward CO (S_{CO}) Measured at the Exit of the XPS Pretreatment Chamber under the Conditions Described in Fig. 2

Reaction temp. (K)	Ru/TiO_2		$Ru/TiO_2(Ca^{2+})$		$Ru/TiO_2(W^{6+})$	
	S_{CO} (%)	X_{CH_4} (%)	S_{CO} (%)	X_{CH_4} (%)	S_{CO} (%)	X_{CH_4} (%)
673	0	8	0	11	0	13
823	50	33	50	35	35	24
973	74	42	81	59	54	28

Yokomizo *et al.* (19), who studied CO adsorption on Ru/SiO_2, attributed a band at 2140 cm^{-1} and a portion of a band at 2080 cm^{-1} to tricarbonyl species bonded on partially oxidized particles, while the remainder of the band at 2080 cm^{-1} was attributed to CO linearly bonded on Ru sites perturbed by adsorbed oxygen atoms.

The FTIR spectra obtained from the Ru/TiO_2 catalyst previously treated with the reaction mixture at 773 and 973 K are presented in Fig. 4A, traces b and c, respectively. These spectra are qualitatively similar to the one obtained over the reduced catalyst (compare with trace a), indicating that Ru remains in its reduced state following treatment at these reaction conditions. This is also evidenced by comparison with the (very different) spectrum obtained from the preoxidized sample, which is characterized by an intense band at 2070 cm^{-1} (trace d).

In addition to the clearly distinguishable bands discussed above, one or more bands might be present in the IR spectra of Fig. 4A, which are responsible for the low-frequency shoulder of the 2043-cm^{-1} band. A portion of this "tail" may be attributed to the low-wavenumber counterpart of the species responsible for the observation of the 2135- and 2070-cm^{-1} peaks. Multicarbonyl species are normally expected to exhibit more than one vibrational bands in the ν(C–O) region unless they are too weak to be observed due to the orientation of the molecular axis of CO with respect to the surface normal (22). For example, $Ru^{n+}(CO)_2$ dicarbonyls are characterized by a pair of bands at 2092–2045 and 2038–1970 cm^{-1} (13), the latter of which lies in the spectral region where the "tail" under discussion is located.

The FTIR spectra obtained from the $Ru/TiO_2(Ca^{2+})$ catalyst are shown in Fig. 4B. As in the case of the undoped catalyst, the spectra obtained from the sample previously treated with the CH_4–O_2 mixture at 773 and 973 K (traces b and c, respectively) are characterized by an intense band due to Ru^0–CO, which is now shifted to ca. 2050 cm^{-1}. Comparison with the spectra obtained following treatment with H_2 (trace a) or O_2 (trace d) shows that, as in the case of the undoped catalyst, under reaction conditions Ru mainly exists in its metallic state.

The corresponding spectra obtained from $Ru/TiO_2(W^{6+})$ are presented in Fig. 4C. In contrast to the undoped and the Ca^{2+}-doped catalysts, spectra obtained following treatment at reaction conditions (traces b and c) are dominated by intense bands at 2142 and 2080 cm^{-1}, which, as discussed above, are characteristic of CO species adsorbed on oxidized sites.

3.4.2. In situ FTIR spectra under reaction conditions. *In situ* FTIR spectra obtained from Ru/TiO_2, $Ru/TiO_2(Ca^{2+})$, and $Ru/TiO_2(W^{6+})$ catalysts under reaction conditions, in the temperature range of 773–1073 K, are presented in Fig. 5A–5C, respectively. In these experiments, the effluent from the IR cell was analyzed by gas chromatography and the results are summarized in Table 4. It is observed

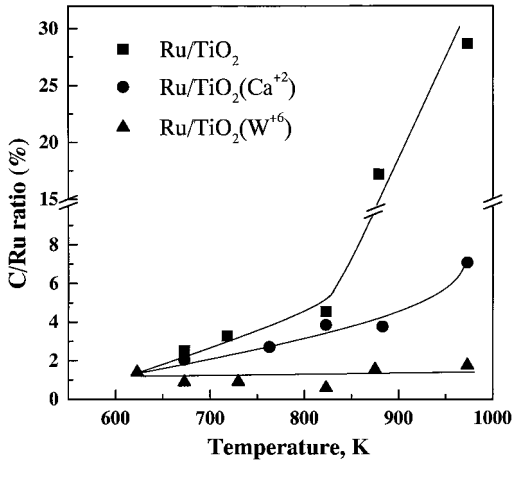

FIG. 3. Dependence of the C/Ru atomic ratios, determined from XPS measurements, on reaction temperature.

TABLE 4

Conversion of Methane (X_{CH_4}) and Selectivity toward CO (S_{CO}) Measured at the Exit of the FTIR Cell under the Conditions Described in Fig. 5

	Ru/TiO_2		$Ru/TiO_2(Ca^{2+})$		$Ru/TiO_2(W^{6+})$	
T_R (K)	S_{CO} (%)	X_{CH_4} (%)	S_{CO} (%)	X_{CH_4} (%)	S_{CO} (%)	X_{CH_4} (%)
773	11	18	8	16	0	6
823	33	20	36	26	7	14
973	59	28	64	36	14	17
1073	67	31	75	41	32	24

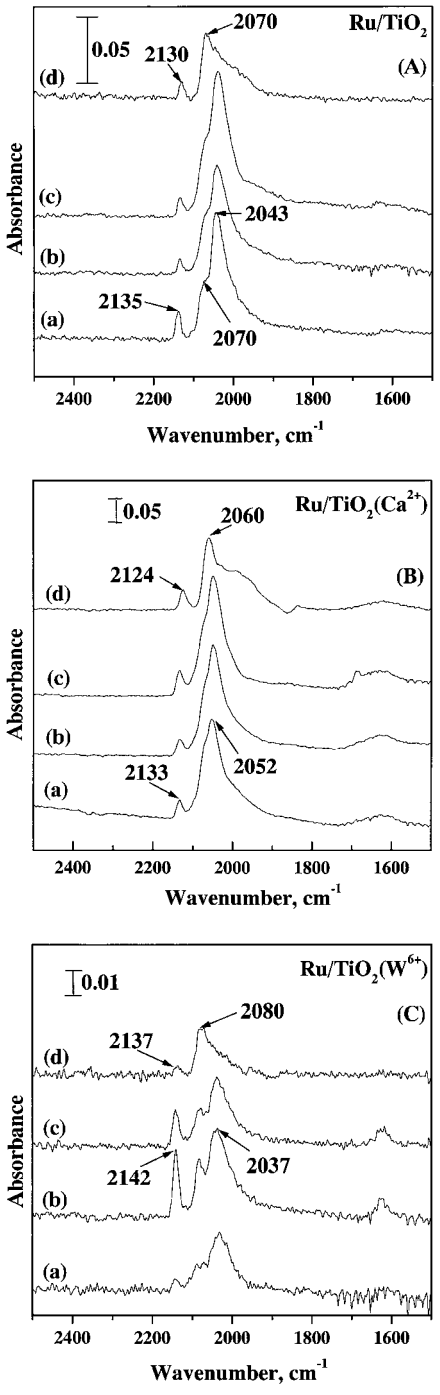

FIG. 4. Spectra of adsorbed CO obtained from (A) Ru/TiO_2, (B) $Ru/TiO_2(Ca^{2+})$, and (C) $Ru/TiO_2(W^{6+})$ catalysts obtained at 300 K after (a) reduction with 20% H_2 (in Ar) at 773 K for 60 min, (b) treatment with 10% CH_4–5% O_2 (in Ar) at 773 K, (c) treatment with the same mixture at 973 K, and (d) oxidation with 7% O_2 at 473 K for 10 min.

that, in the case of Ru/TiO_2, interaction of the 10% CH_4–5% O_2 (in Ar) mixture with the reduced catalyst at 773 K gives rise to FTIR bands due to gas-phase CH_4 (3250–2750 cm^{-1}), to gas-phase CO_2 (2360/2340 cm^{-1}), and to a broad band at ca. 1985 cm^{-1} (Fig. 5A). Although bands due to gas phase CO (2180/2100 cm^{-1}) are not present at this reaction temperature, analysis of the effluent gas at the exit of the FTIR cell shows that there was CO production (Table 4). The absence of the corresponding bands may be attributed to the relatively low concentration of CO in the gas phase.

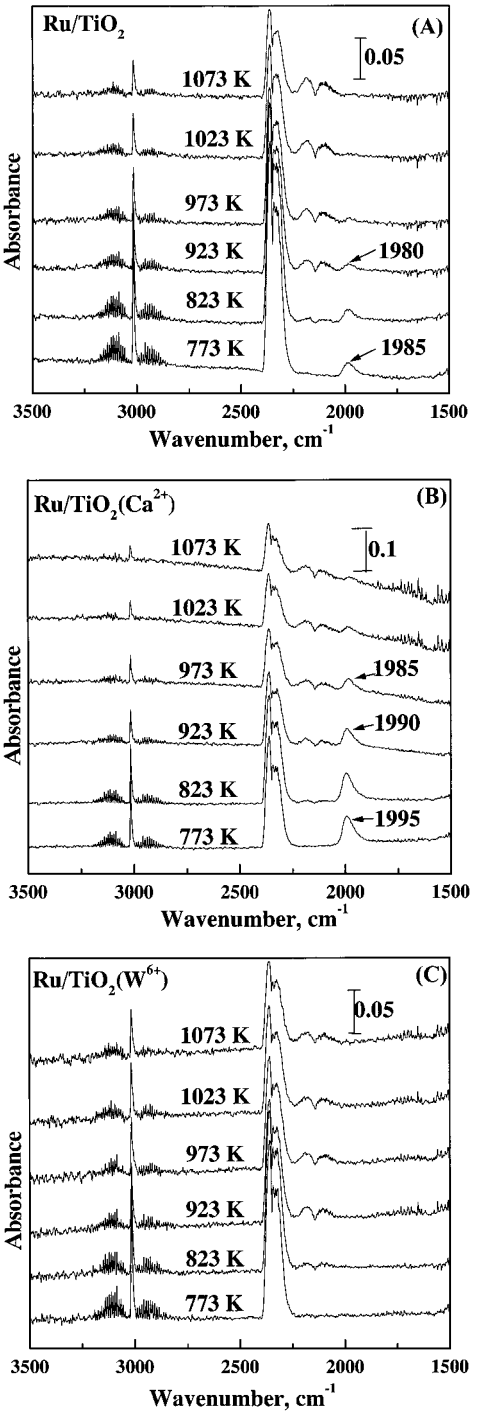

FIG. 5. *In situ* FTIR spectra obtained from (A) Ru/TiO_2, (B) $Ru/TiO_2(Ca^{2+})$, and (C) $Ru/TiO_2(W^{6+})$ catalysts during interaction with flowing 10% CH_4–5% O_2 (in Ar) mixture in the temperature range of 773–1073 K.

Increasing reaction temperature to 823 K results in the appearance of bands due to gas phase CO, located at around 2180 and 2100 cm^{-1}, which continuously increase in intensity with increasing temperature, up to 1073 K (Fig. 5A). At the same time, the bands due to gas phase CO_2 and CH_4 decrease in intensity. This implies increased methane conversions and increased selectivities toward CO, which is confirmed by GC analysis (Table 4). The 1985-cm^{-1} band decreases in intensity and shifts toward lower frequencies with increasing reaction temperature and can be hardly observed at temperatures above 973 K.

The spectra obtained from the Ca^{2+}-doped sample (Fig. 5B) are qualitatively similar to the corresponding ones obtained over the undoped catalyst and are also characterized by a band in the spectral region where adsorbed CO species are expected to absorb. This band, which is now located at ca. 1995 cm^{-1}, is of much higher intensity compared to the one observed over the undoped catalyst (note the difference in the scale of the *y* axis). In addition, the corresponding species can be clearly observed at reaction temperatures as high as 1073 K (Fig. 5B). The peak maximum gradually shifts toward lower frequencies upon increasing reaction temperature above 923 K.

In contrast to the undoped and Ca^{2+}-doped catalysts, no bands are observable in the 2000- to 1950-cm^{-1} region over the W^{6+}-doped catalyst, even at low reaction temperatures (Fig. 5C). Again, this catalyst is much less active and selective compared to the undoped and Ca^{2+}-doped ones, the latter exhibiting the best catalytic behavior (Table 4).

4. DISCUSSION

4.1. Effect of Carrier Doping on the Catalytic Performance of Ru

As observed in Fig. 1 and Table 2, under experimental conditions where oxygen is not fully consumed ($X_{CH_4} < 35\%$), selectivities of Ru-containing catalysts toward CO and H_2 formation strongly depend on the nature of the supporting material. It must be noticed that, as long as there is oxygen present in the gas phase, the contribution of CH_4-reforming reactions (steam and CO_2 reforming) is very small and, therefore, formation of CO and H_2 takes place mainly via the direct route of partial oxidation of CH_4 (12).

Additional indication that the direct route is operable comes from the experimental conditions employed, of which space velocity is of great importance. When the partial oxidation of methane proceeds via the indirect scheme, it is expected that selectivities toward CO and H_2 will decrease with increasing space velocity (9, 23, 24). The constant selectivities observed in the present study with variation of space velocity (results not shown) imply that CO and H_2 are the primary products of the reaction. The theory of primary formation of CO and H_2 at low methane conversions has recently been strengthened by a kinetic model, which satisfies very nicely the experimental results (25).

It may be concluded that, under conditions where the direct route is operable ($X_{CH_4} < 35\%$), doping of TiO_2 with Ca^{2+} results in enhancement of the reactions that lead toward CO and H_2 formation, while the opposite is true upon doping with W^{6+} cations. The fact that the values of S_{CO} and S_{H_2} remain constant as long as there is oxygen in the gas phase ($X_{CH_4} < 35\%$, Fig. 1) implies that the Ru surface remains unchanged with respect to the percentage of the active sites that are responsible for the direct route of partial oxidation of methane for each one of the catalysts examined.

Regarding the nature of the catalytically active sites, results of published work indicate that the reduced metallic sites are mainly involved in CH_4 activation and synthesis gas formation (9, 26–28). Theoretical calculations (29) and experimental results (30) have shown that the rate of CH_4 adsorption increases over catalyst surfaces containing very little surface oxygen or when oxygen is located at metal "on top" sites. In all cases, the presence of reduced sites seems to be necessary for the reaction to proceed.

Since all experiments presented in Fig. 1 have been conducted under similar experimental conditions, the differences observed in the catalytic performance may be attributed to the effect of modification of the supporting material on one or more critical properties of the Ru crystallites.

4.2. The Oxidation State of Supported Ru Crystallites under CPO Reaction Conditions

4.2.1. Effect of reaction temperature. XPS results of the present study clearly show that the oxidation state of ruthenium depends on reaction temperature; i.e., the percentage of metallic Ru in the ruthenium crystallites increases with increasing reaction temperature, as is clearly demonstrated in Figs. 2A–2C for all three catalysts examined. The enhancement of the reduced fraction of the Ru with temperature is accompanied by enhancement of selectivity of CO and H_2 production in the presence of oxygen (Table 2) and by an increase of the amount of surface carbon that accumulates under reaction conditions, as indicated by the C/Ru atomic ratios, which are shown in Fig. 3. These observations may be explained as follows: At the lower reaction temperature of 673 K where the catalyst is partially oxidized (Fig. 2), the Ru surface is almost fully covered with oxygen because the competitive adsorption between oxygen and a saturated hydrocarbon like CH_4 strongly favors oxygen under the particular experimental conditions. This is due to the fact that, methane, which is a thermodynamically stable molecule, has a low sticking coefficient at low temperatures (31), especially when a portion of the surface is covered by adsorbed oxygen species (32, 33). This is the case for all three catalysts

examined. Thus, considering CH_4 dissociative adsorption as the rate-limiting step, the production of CO_2, with selectivity approaching 100% at temperatures lower than 673 K, can be attributed to the significantly higher activity of the oxidized catalysts toward combustion of adsorbed species, which result from the dissociative adsorption of CH_4. Alternatively stated, at low reaction temperatures the competition between CH_4 and oxygen for interaction with Ru favors the latter, resulting in an oxidized Ru surface, which leads toward CO_2 and H_2O formation.

When the reaction temperature is increased, the dissociation probability of CH_4 increases (30, 31) and so does the reaction probability, which is evidenced by the higher CH_4 conversions observed (Table 3). At 823 K, this is accompanied by reduction of the Ru surface (Fig. 2) and the appearance of CO in the gas phase (Table 3). It must be noticed that the contribution of CH_4-reforming reactions (CO_2 and H_2O) to the total CO production is negligible. The fact that reforming reactions contribute negligiblly to CO and H_2 production has been established in our detailed kinetic study (25) and is supported by the observations of low CH_4 conversions at 823 K (Table 3) and the fact that the C/Ru atomic ratios do not change significantly with temperature in this temperature range (Fig. 3).

A definite correlation exists between the oxidation state of the Ru crystallites, as observed by XPS (Fig. 2b–d), and selectivity toward CO and H_2 formation at low CH_4 and O_2 conversions (Fig. 1). The high CO and H_2 selectivities observed over the undoped and Ca^{2+}-doped catalysts may be attributed to the ability of the corresponding carriers to stabilize the Ru crystallites mainly in their metallic state in the presence of oxygen in the gas phase. In contrast, on the W^{6+}-doped catalyst, a large fraction of the Ru crystallites exist in the oxidized state, which results in reduced selectivity toward CO and H_2 formation via the direct route.

The dissociation probability of CH_4 becomes comparable to the reaction rate of the oxidation processes with increasing catalyst temperature. This is accompanied by further reduction of the Ru surface (Fig. 2), the depletion of surface oxygen, and the enhanced production of CO and H_2. As shown in Table 3, at temperatures above 900 K CH_4 conversion exceeds 35% and the C/Ru ratio is increased in the case of the undoped and Ca^{2+}-doped catalysts (Fig. 3). These observations clearly indicate the onset of CO_2- and H_2O-reforming reactions. It is quite remarkable that, in the case of the Ca^{2+}-doped catalyst, under the same conditions of temperature and CH_4 conversion, the C/Ru ratio is significantly lower compared to that of the Ru/TiO_2 catalyst, while the XP spectra (Fig. 2B, c, d) indicate the existence of CH_x species on the catalyst surface, evidenced by the binding energy of the C(1*s*) peak at 285.2 $\pm$ 0.2 eV (16, 17). Based on these considerations, it may be concluded that the undoped Ru/TiO_2 catalyst is very active toward CH_4 dissociative adsorption, resulting in the formation of graphitic carbon at high reaction temperatures and CH_4 conversions. In contrast, the existence of carbon in the form of CH_x on the Ca^{2+}-doped sample implies that the dissociation rate of CH_4 is lower than the rate of carbon consumption and that the surface is covered mainly with CH_x species. In the case of the W^{6+}-doped catalyst, a considerable part of the Ru crystallites remains in its oxidized form (Fig. 2C). This is the reason for the low CH_4 conversions that have been observed (Table 3) and the lower activity, by 1 order of magnitude, of this catalyst (Table 2).

4.2.2. Effect of carrier doping. XPS (Fig. 2) and FTIR (Fig. 4) results show that under the same reaction conditions the oxidation state of Ru depends on the supporting material. In particular, it is observed that a significant portion of the surface of Ru crystallites dispersed on W^{+6}-doped TiO_2 becomes oxidized, in contrast to the other two catalysts in which the Ru mainly exists in its metallic state. Correlation of this observation with the results of catalytic performance, which are listed in Tables 3 and 4, provides significant evidence that catalytic activity and selectivity may be related to the oxidation state of ruthenium, which in turn, is influenced by altervalent cation doping of the support.

The influence of the support on the electronic state and, consequently, on catalytic properties of supported metal particles has been the subject of extensive research work (34–37) and it is widely accepted that the oxidation state of a supported metal catalyst can be strongly influenced by the interaction of the metal with the carrier. Charge transfer in metal catalysts supported on a TiO_2 carrier has been proposed by many investigators to account for the observed differences in the adsorptive and catalytic properties of the supported metal particles (34–36). Electron transfer from the support to the metal has been proposed in the case of Ru catalysts supported on 19 different kinds of oxides (37). The adsorptive and catalytic behavior of Ru was correlated with the electronegativity of the support, which is a measure of its electron-donating properties.

Regarding the present catalysts, the effect of altervalent cation doping of TiO_2 on the adsorptive and catalytic properties of supported metal catalysts has also been investigated (38–41). It has been shown that doping TiO_2 with higher valence cations than that of the host cation (e.g., W^{6+}) leads to an increase of the *n*-type semiconductivity of the metal oxide, while the opposite is expected for the lower valence cation (e.g., Ca^{2+}) doping. In the case of doped TiO_2, such a metal–support interaction has been established by theoretical analysis (42) and experimental observations (38–40). It has been proposed that a significant charge transfer can occur at the interface of a Group VIII metal and TiO_2 when TiO_2 is either reduced or doped with higher valence cations. The magnitude of charge transfer depends on the metal particle size and can be as high as 0.5 electrons per metal atom for crystallites smaller than 2

nm or less than 0.01 electrons per metal atom for crystallites larger than 10 nm (42).

Based on the theories presented above, since metal crystallites may be viewed as electron donors while the adsorbed oxygen molecules behave as surface electron acceptors, it is expected that, in the case of the W^{6+}-doped catalyst, where charge transfer from the carrier to the supported Ru is increased, the oxygen chemisorption process will be favored. In addition, doping TiO_2 with W^{6+} cations will also favor the formation of active oxygen species, such as O_2^-, O_2^{2-}, and O^-, which are generated by electron acceptance on the metal surface (43). Therefore, the stabilization of Ru in its oxidized forms observed over the W^{6+}-doped catalyst under reaction conditions (Figs. 2C, 4C) may be attributed to the stronger interaction of oxygen with the Ru surface compared to those of the other two catalysts, which originates from the W^{6+}-induced increase of charge transfer from the carrier to the Ru crystallites.

The opposite behavior is expected from the Ca^{2+}-doped catalysts under similar experimental conditions; i.e., Ru should remain in the metallic state under reaction conditions and should be more easily reduced compared to the undoped catalyst. This is because according to the above discussion, doping TiO_2 with Ca^{2+} cations results in reduced charge transfer to the Ru crystallites. Thus, it is expected that Ru on Ca^{2+}-doped TiO_2 will exhibit lower electron availability at the Fermi level. Under these conditions the origin and nature of the surface species detected is expected to be significantly affected, thus leading to the differences in reaction rates and selectivities observed over the three Ru catalysts (Table 2).

4.3. Nature and Origin of Surface Species Detected under Reaction Conditions

As observed in Fig. 5, the only IR band observed under reaction conditions, which is attributable to adsorbed CO species, is the one located at 1985 (or 1995) cm^{-1} over the undoped (or Ca^{2+}-doped) catalyst. This peak appears at relatively low frequency, which indicates (a) very low surface coverage of the corresponding adsorbed CO species and/or (b) adsorption on very small or isolated Ru sites and/or (c) the presence of an electron donor in the vicinity of the adsorption sites.

Regarding the effect of surface coverage, it has been reported that adsorption of CO on Ru(001) single crystals results in the appearance of a single-frequency band due to linearly bonded CO on reduced sites, shifting from 1984 to 2060 cm^{-1} with increasing CO coverage from 0.003 to 0.66 (44). Shifts of similar magnitude were observed by Kellner and Bell over Ru/Al_2O_3 catalysts (45). However, the highest and the lowest frequencies reported in that study were notably lower than those on single crystals, a result which was partly attributed to differences between the physical properties of alumina-supported Ru microcrystallites and bulk Ru metal (45). It is reasonable to assume that, under the high-temperature reaction conditions employed here, only low coverages of strongly adsorbed CO will be present on the catalyst surface and participate in surface reactions.

The morphology and crystallite size of Ru may also determine the exact band position of adsorbed CO (46). Bands in the spectral region where the 1985- (or 1995-) cm^{-1} peak is observed are characteristic of CO adsorbed on high-index faces where CO adsorbs more strongly than that on a flat surface (47). This is supported by the fact that adsorption of CO on well-dispersed catalysts results in lower frequency bands compared to the corresponding ones over sintered catalysts (47). As has been discussed in our previous study (13), spectral features located below 2020 cm^{-1} may be due to CO adsorption on isolated Ru^0 entities of very low nuclearity and/or to Ru^0–CO species "diluted" in an oxidized environment.

As mentioned earlier, the various dopants modify the TiO_2 support, altering significantly the electronic properties of the Ru crystallites. CO is adsorbed on top of Ru^0 by donating electrons from the 5σ orbital to the metal *d* band (48) with concomitant backdonation of electrons to the $2\pi^*$ level, thus affecting the C=O bond. Therefore, it is expected that the C–Ru bond will be stronger on the Ca^{2+}-doped catalyst. However, the C=O bond of the adsorbed CO molecules on Ru crystallites will be less affected on the Ca^{2+}-doped catalyst as compared to that on the undoped one. The above conclusions are supported by the IR spectra (Figs. 5A and 5B), which show that CO coverage under reaction conditions is larger on the Ca^{2+}-doped catalyst while the CO stretching frequency has the highest value among the three catalysts, denoting stronger bonding between the carbon and oxygen. Thus, both CO coverage and C=O stretching frequency increase in the order $TiO_2(W^{6+}) < TiO_2 < TiO_2(Ca^{2+})$, denoting stronger bonding with the Ru surface supported on $TiO_2(Ca^{2+})$ and weaker interaction of the C=O bond with the catalyst surface.

The low frequency of the 1985- (1995-) cm^{-1} band may also be related to the presence of species like hydrogen and/or carbon in the vicinity of the adsorption sites. From various studies concerning interaction of CO + H_2 over supported Ru catalysts (20, 49, 50), IR bands observed at around 1990 cm^{-1} were attributed to the formation of ruthenium carbonyl hydrides of the following type:

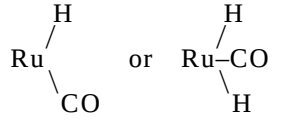

Formation of ruthenium carbonyl hydrides produced through the dehydrogenation of methane could also explain the low vibrational frequencies observed in the present

study (7):

$$CH_4 + Ru \rightarrow CH_x - Ru \xrightarrow{O_S} Ru\begin{matrix}\diagup CO \\ \\ \diagdown H\end{matrix} \quad \text{or} \quad \begin{matrix}H \\ | \\ Ru\text{–}CO \\ | \\ H\end{matrix} \qquad [1]$$

The influence of surface carbon on the vibrational frequency of adsorbed CO species was supported by Dalla Betta and Shelef (50) and Kellner and Bell (45), who assigned bands at frequencies lower than 2000 cm^{-1} to CO adsorbed in a linear mode at a Ru site adjacent to a nucleophilic adsorbate, such as carbon.

In the present case, surface carbon formed under reaction conditions could be responsible for the observed low frequency of adsorbed CO species (Figs. 5A and 5B). If that was the case, one would expect to observe a shift of the band position toward lower frequencies with increasing concentration of the surface carbon, especially at high CH_4 conversions ($X_{CH_4} > 35\%$), where oxygen is fully consumed and, therefore, carbon deposition is favored. This is clearly shown in the case of the Ca^{2+}-doped catalyst (Fig. 5B), where a shift of ca. 10 cm^{-1} is observed with increasing temperature above 923 K where the CH_4 conversion is above 35%. It should be noted that part of this shift could be attributed to the decrease in the surface coverage of this species, which takes place upon increasing reaction temperature.

In view of the previous discussion, it may be concluded that the IR peak located at 1985 (or 1990) cm^{-1}, which is observed over the undoped and Ca^{2+}-doped samples at reaction conditions, is due to CO species linearly bonded on reduced Ru sites. The low frequency of this peak is due to the low surface coverage of the corresponding species. Assuming that there are no significant differences in the morphological characteristics of the three catalysts examined under reaction conditions, such as structural arrangements of the Ru crystallites, it is reasonable to suggest that the presence and population of this adsorbed CO species depends on the oxidation state and the electronic properties of the catalyst, which in turn, depend on the type of the support employed to disperse the Ru crystallites, in particular, the type of doping cation incorporated into the crystal matrix of TiO_2.

It is generally accepted that the dissociative adsorption of methane is significantly favored on metal surfaces with a high Fermi level (48). The dissociation of the C–H bond depends on the strong backdonation of electrons into the antibonding of the stretched C–H bond. Thus, it is reasonable to consider that the CH_x species, shown in the XP spectra in Fig. 2, can be more stable on the Ca^{2+}-doped catalyst since the electron transfer at $Ru/TiO_2(Ca^{2+})$ is less among the three catalyst systems examined. In contrast, in the case of the Ru/TiO_2 catalyst, the production of graphitic carbon is prevailing at high temperatures and CH_4 conversions. Although the W^{6+}-doped catalyst should exhibit even higher carbon accumulation, the low methane conversions and the highly oxidizing environment (partially oxidized catalyst and gas phase oxygen) maintains carbon at a low level.

4.4. Mechanistic Implications

Results of the present study may be related to our recent work in which the kinetic behavior of the $Ru/TiO_2(Ca^{2+})$ catalyst in the partial oxidation of methane to synthesis gas was investigated and a kinetic model was developed (25). According to this model, CO and H_2 are the primary reaction products while CO_2 and H_2O are secondary oxidation products. Methane adsorbs dissociatively and irreversibly on specific surface sites (designated as S_1) toward the formation of surface carbon and adsorbed hydrogen atoms:

$$CH_4 + S_1 \rightarrow I \rightarrow C\text{–}S_1 + 4H\text{–}S_1. \qquad [2]$$

Results of the present study indicate that "S_1" are reduced Ru sites, which is in accordance with the findings in the literature (9, 26–28).

Regarding the formation of CO and CO_2, it was proposed that the former is a primary product of the reaction between surface carbon and oxygen and that adsorbed CO is at equilibrium with gas phase CO (25):

$$C\text{–}S_1 + O\text{–}S_2^* \rightarrow CO\text{–}S_1 + S_2^* \qquad [3]$$

$$CO + S_1 \leftrightarrow CO\text{–}S_1. \qquad [4]$$

It must be noticed that in the elementary step (3) the S_2^* sites originate from the interaction of gas phase oxygen with the surface sites S_2, which are assumed to be different from the S_1 sites. The surface sites S_2 constitute the active region for carbon dioxide production via subsequent oxidation of CO, following its readsorption on these surface sites (S_2):

$$CO + S_2 \leftrightarrow CO\text{–}S_2 \qquad [5]$$

$$CO\text{–}S_2 + O\text{–}S_2^* \rightarrow CO_2 + S_2 + S_2^*. \qquad [6]$$

It is of interest to notice that the above model predicts that CO coverage decreases with increasing temperature, as expected from adsorption thermodynamics and that, under the experimental conditions applied in the *in situ* FTIR experiments of Fig. 5, CO coverage is ca. 0.05 at 973 K and ca. 0.01 at 1073 K (25). This explains the appearance of the FTIR band due to adsorbed CO species under such high reaction temperatures.

In view of the *in situ* FTIR results of the present study (Fig. 5), it is tempting to correlate the adsorbed CO species of the above kinetic model (namely, $CO\text{–}S_1$) with the FTIR peak observed under reaction conditions. It may be assumed that this peak corresponds to an adsorption site where CO can accumulate and desorb (Eq. [4]). Moreover,

it could be assumed that the dissociation of CH_4 and the production of CO take place in the same surface-active sites S_1. An indication that supports the assumption of CH_4 dissociation and the adsorption of CO at the same active site is the frequency shift of the peak when the conditions are favorable for carbon deposition (Fig. 5). The absence of adsorbed oxygen on adjacent sites allows desorption of CO without further oxidation at these sites.

The appearance and relative intensity of the 1985- (1995-) cm^{-1} peak under reaction conditions may be related to the catalytic performance of the Ru catalysts examined. As observed in Fig. 5, this band is present over the undoped and Ca^{2+}-doped catalysts, which are highly active and selective toward synthesis gas formation and over which the metal mainly exists in its reduced form. The high selectivity obtained over these catalysts strengthens the view that these species survive and desorb from the catalyst surfaces without being further oxidized. In contrast, over the W^{6+}-doped catalyst, which is much less active and selective and which under reaction conditions mainly exists in oxidized forms, such IR bands are absent.

5. CONCLUSIONS

The following conclusions may be drawn from the results of the present study:

1. Under conditions where the direct route for the partial oxidation of methane to synthesis gas formation is operable ($X_{CH_4} < 35\%$), the catalytic performance of Ru/TiO_2 catalysts is improved upon doping of TiO_2 with small amounts of Ca^{2+} cations, while the opposite is true upon doping with W^{6+} cations.

2. The oxidation state of ruthenium depends strongly on the reaction temperature and, under reaction conditions, the fraction of metallic Ru increases with increasing temperature. This is accompanied by increased selectivities toward CO and H_2 formation, indicating that Ru(0) sites are necessary for the reaction to proceed.

3. Altervalent cation doping of TiO_2 results in significant changes in the oxidation state of supported Ru, which is reflected in its catalytic performance. In particular, doping with W^{6+} cations results in the stabilization of a portion of Ru in its oxide forms under reaction conditions and, concomitantly, in lower methane conversions and lower selectivities toward CO and H_2 formation compared to the undoped catalyst. In contrast, doping of the carrier with Ca^{2+} cations results in stabilization of Ru in its metallic form and, thus, to enhanced catalytic performance with respect to activity and selectivity for CO and H_2 formation.

4. *In situ* FTIR results show that an adsorbed CO species exists on the surface of the undoped and Ca^{2+}-doped catalysts under reaction conditions, even at temperatures as high as 1073 K. This species, which is not observable over the W^{6+}-doped catalyst, may be related to an adsorption site that seems to be necessary for the reaction to proceed.

REFERENCES

1. Pena, M. A., Gomez, J. P., and Fierro, J. L. G., *Appl. Catal. A* **144**, 7 (1996).
2. Mallens, E. P. J., Hoebink, J. H. B. J., and Marin, G. B., *J. Catal.* **167**, 43 (1997).
3. Fathi, M., Monnet, F., Schuurman, Y., Holmen, A., and Mirodatos, C., *J. Catal.* **190**, 439 (2000).
4. Buyevskaya, O. V., Walter, K., Wolf, D., and Baerns, M., *Catal. Lett.* **38**, 81 (1996).
5. Torniainen, P. M., Chu, X., and Schmidt, L. D., *J. Catal.* **146**, 1 (1994).
6. Qin, D., Lapszewicz, J., and Jiang, X., *J. Catal.* **159**, 140 (1996).
7. Tian, Z., Dewaele, O., and Marin, G. B., *Catal. Lett.* **57**, 9 (1999).
8. Soick, M., Buyevskaya, O. V., Höhenberger, M., and Wolf, D., *Catal. Today* **32**, 163 (1996).
9. Dissanayake, D., Rosynek, M. P., Kharas, K. C. C., and Lunsford, J. H., *J. Catal.* **132**, 117 (1991).
10. Hu, Y. H., and Ruckenstein, E., *J. Catal.* **158**, 260 (1996).
11. Boucouvalas, Y., Zhang, Z. L., Efstathiou, A. M., and Verykios, X. E., *Stud. Surf. Sci. Catal.* **101**, 443 (1996).
12. Boucouvalas, Y., Zhang, Z. L., and Verykios, X. E., *Catal. Lett.* **40**, 189 (1996).
13. Elmasides, C., Kondarides, D. I., Grüenert, W., and Verykios, X. E., *J. Phys. Chem. B* **103**, 5227 (1999).
14. Fuggle, J. C., Madey, T. E., Steinkilberg, M., and Menzel, D., *Surf. Sci.* **52**, 521 (1975).
15. Chan, H. Y. H., Takoudis, C. G., and Weaver, J., *J. Catal.* **172**, 336 (1997).
16. Johnson, E. E., and Ratner, B. D., *J. Electron Spectrosc. Related Phenom.* **81**, 303 (1996).
17. Sabbatini, L., and Zambonin, P. G., *J. Electron Spectrosc. Related Phenom.* **81**, 285 (1996).
18. Hadjiivanov, K., Lavalley, J. C., Lamotte, J., Maugé, F., Saint-Just, V., and Che, M., *J. Catal.* **176**, 415 (1998).
19. Yokomizo, G. H., Louis, C., and Bell, A. T., *J. Catal.* **120**, 1 (1989).
20. Gupta, N. M., Kamble, V. S., Iyer, R. M., Ravindranathan Thampi, K., and Gratzel, M., *J. Catal.* **137**, 473 (1992).
21. Robbins, J. L., *J. Catal.* **115**, 120 (1989).
22. Chen, H. W., Zhong, Z., and White, J. M., *J. Catal.* **90**, 119 (1984).
23. Van Looij, F., van Giezen, J. C., Stobbe, E. R., and Geus, J. W., *Catal. Today* **21**, 495 (1994).
24. Nakagawa, K., Ikenaga, N., Suzuki, T., Kobayashi, T., and Haruta, M., *Appl. Catal. A* **169**, 281 (1998).
25. Elmasides, C., Ioannides, T., and Verykios, X. E., *AIChE J.* **46**, 1260 (2000).
26. Wang, D., Dewaele, O., De Groote, A. M., and Froment, G. F., *J. Catal.* **159**, 418 (1996).
27. Au, C. T., and Wang, H. Y., *J. Catal.* **167**, 337 (1997).
28. Wang, H. Y., and Ruckenstein, E., *Catal. Lett.* **59**, 121 (1999).
29. Au, C-T., Liao, M-S., and Ng, C-F., *J. Phys. Chem. A* **102**, 3959 (1998).
30. Wang, D., Dewaele, O., and Froment, G. F., *J. Mol. Catal. A* **136**, 301 (1998).
31. Koerts, T., Deelen, M. J. A. G., and van Santen, R. A., *J. Catal.* **138**, 101 (1992).
32. Valden, M., Xiang, N., Pere, J., and Pessa, M., *Appl. Surf. Sci.* **99**, 83 (1996).
33. Valden, M., Pere, J., Xiang, N., and Pessa, M., *Chem Phys. Lett.* **257**, 289 (1996).
34. Belton, D. N., Sun, Y. M., and White, J. M, *J. Phys. Chem.* **88**, 5172 (1984).
35. Solymosi, F., Tombacz, I., and Kocsis, M., *J. Catal.* **75**, 78 (1982).

36. Raupp, G. B., and Dumesic, J. A., *J. Catal.* **97**, 85 (1986).
37. Ishihara, T., Harada, K., Eguchi, K., and Arai, H., *J. Catal.* **136**, 161 (1992).
38. Akubuiro, E. C., and Verykios, X. E., *J. Catal.* **103**, 320 (1987).
39. Zhang, Z., Kladi, A., and Verykios, X. E., *J. Phys. Chem*. **98**, 6804 (1994).
40. Solymosi, F., Tombacz, I., and Koszta, J., *J. Catal.* **95**, 578 (1985).
41. Zhang, Z., Verykios, X. E., and Baerns, M., *Catal. Rev.-Sci. Eng.* **36**(3), 507 (1994).
42. Ioannides, T., and Verykios, X. E., *J. Catal.* **161**, 560 (1996).
43. Sokolovskii, V. D., *Catal. Rev.-Sci. Eng.* **32**, 1 (1990).
44. Pfnur, H., Menzel, D., Hoffman, F., Ortega A., and Bradshaw, A. M., *Surf. Sci.* **93**, 431 (1980).
45. Kellner, C. S., and Bell, A. T., *J. Catal.* **71**, 296 (1981).
46. Dalla Betta, R. A., *J. Phys. Chem*. **79**, 2519 (1975).
47. Guglielminotti, E., Spoto, G., and Zecchina, A., *Surf. Sci.* **161**, 202 (1985).
48. Van Santen, R. A., and Neurock, M., *Catal. Rev.-Sci. Eng.* **37**, 557 (1995).
49. Solymosi, F., Tombacz, I., and Kocsis, M., *J. Catal.* **75**, 78 (1982).
50. Dalla Betta, R. A., and Shelef, M., *J. Catal.* **48**, 111 (1977).